

University of Groningen

Concentrated Multi-nozzle Electrospinning

Zheng, Yuekun; Cao, Huatang; Zhou, Zhou; Mei, Xuecui; Yu, Lingke; Chen, Xiaojun; He, Gonghan; Zhao, Yang; Wu, Dezhi; Sun, Daoheng

Published in:
Fibers and Polymers

DOI:
[10.1007/s12221-019-8984-y](https://doi.org/10.1007/s12221-019-8984-y)

IMPORTANT NOTE: You are advised to consult the publisher's version (publisher's PDF) if you wish to cite from it. Please check the document version below.

Document Version
Publisher's PDF, also known as Version of record

Publication date:
2019

[Link to publication in University of Groningen/UMCG research database](#)

Citation for published version (APA):

Zheng, Y., Cao, H., Zhou, Z., Mei, X., Yu, L., Chen, X., He, G., Zhao, Y., Wu, D., & Sun, D. (2019). Concentrated Multi-nozzle Electrospinning. *Fibers and Polymers*, 20(6), 1180-1186. <https://doi.org/10.1007/s12221-019-8984-y>

Copyright

Other than for strictly personal use, it is not permitted to download or to forward/distribute the text or part of it without the consent of the author(s) and/or copyright holder(s), unless the work is under an open content license (like Creative Commons).

The publication may also be distributed here under the terms of Article 25fa of the Dutch Copyright Act, indicated by the "Taverne" license. More information can be found on the University of Groningen website: <https://www.rug.nl/library/open-access/self-archiving-pure/taverne-amendment>.

Take-down policy

If you believe that this document breaches copyright please contact us providing details, and we will remove access to the work immediately and investigate your claim.

Downloaded from the University of Groningen/UMCG research database (Pure): <http://www.rug.nl/research/portal>. For technical reasons the number of authors shown on this cover page is limited to 10 maximum.

Concentrated Multi-nozzle Electrospinning

Yuekun Zheng¹, Huatang Cao², Zhou Zhou¹, Xuecui Mei¹, Lingke Yu¹, Xiaojun Chen¹, Gonghan He¹,
Yang Zhao¹, Dezhi Wu¹, and Daoheng Sun^{1*}

¹Department of Mechanical and Electrical Engineering, Xiamen University, Xiamen 361005, China

²Department of Advanced Production Engineering, Faculty of Science and Engineering, University of Groningen,
Nijenborgh 4, 9747AG, The Netherlands

(Received October 18, 2018; Revised January 8, 2019; Accepted January 11, 2019)

Abstract: The multi-nozzle electrospinning is under extensive investigations because it is an easy way to enhance the productivity and also feasible to produce special structure fibers such as core-shell fibers and to fabricate composite fibers of those polymers that cannot form blend solution in common solvent. Control over the multi-nozzle electrospinning fibers deposition has attracted increasing attentions. The most common method was to use the auxiliary electrode. However, the concentrated effect of the works of control multi-nozzle electrospinning deposit was inconspicuous. To enhance the controlling of multi-nozzle electrospinning deposition, a set-up based oppositely charged electrospinning was designed. In this set-up the air flow was used to transport neutralized nanofibers. This electrospinning method was named oppositely charged and air auxiliary electrospinning (OCAAES). The capacity of OCAAES in deposition area and pattern controlling were investigated. By the OCAAES, concentrated and several patterned nanofibers deposition were fabricated. Results showed that nanofiber deposition area and pattern of multi-nozzle electrospinning could be controlled actively, and nanofiber deposition could be fabricated in a quick thickening rate.

Keywords: Multi-nozzle electrospinning, Nanofiber, Oppositely charged, Air flow, Concentrated

Introduction

Electrospinning is a straightforward process to produce nanofibers with diameters ranging from around 3 nm to 2 μm through an electrically charged jet of polymer solution or polymer melt. Nanofibers possess unique features such as high porosity with interconnected porous structure and small pore size, biocompatible, tunable surface functionalities [1,2], therefore they find their applications in various fields such as bio-scaffolds [3-5], filtrations [6-10], and separator of lithium-ion batteries [11,12]. However, the widespread industrial applications of this technique are primarily limited by its low production rate about 0.01-1 g/h from a single jet electrospinning process. In recent years, some methods such as multi-nozzle electrospinning [13-18] and free surface electrospinning [19-21] have been developed to increase the production rate of the electrospun nanofibers. Although most of the free surface electrospinning could fabricate nanofiber at a relatively high production rate, the multi-nozzle electrospinning is still under extensive investigation, since it is not only an easy way to enhance the productivity but also a simple technique to produce complex structure fibers such as core-shell fibers and to fabricate composite fibers of those polymers that cannot form blend solution in common solvent [22]. One main disadvantage of the multi-nozzle system, however, is the mutual repulsion from the adjacent jets which increases the difficulty in nanofibers collecting.

Control over the multi-nozzle electrospinning fibers deposition has attracted increasing attentions. To control multi-nozzle electrospinning deposition on a relatively small and concentrated area, the most common method was to use the auxiliary electrode. Kim *et al.* designed an electrospinning process with a cylindrical auxiliary electrode to stabilize the initially spun solution and control the spun jets deposition area [14]. Yang *et al.* designed a novel system using a PVC insulator tube to introduce an auxiliary electric field and control the jet path [23,24]. Xie *et al.* [25] demonstrated a multi-nozzle spinneret with auxiliary plate and confirmed a higher convergence of the electric field to the spinning line as compared with that of the process without the auxiliary plate. Consequently, a more concentrated fiber mat was collected with the use of the auxiliary plate. Zheng *et al.* [18] designed a two-step spinneret to create larger and more uniform electric field distribution such that the close proximity nanofiber mat was fabricated.

However, the concentrated effect of the previous works of control multi-nozzle electrospinning deposition was insignificant. There is not yet an effective electrospinning setup to fabricate continuous nanofibers mat of multi-nozzle electrospinning, and the deposition area could not be controlled actively. To obtain a better control on the multi-nozzle electrospinning, other new methods were required. Oppositely charged electrospinning (namely, conjugate electrospinning) is a process that uses two opposite polarities of high electrical voltage to form an electric field, and meanwhile uses airflow or mechanical force to control the shape of collected nanofibers. Till now there are already some studies on the oppositely charged electrospinning. Some of nanofiber yarn,

*Corresponding author: sundh@xmu.edu.cn

such as twisted PAN nanofiber yarns [26-28], $[\text{Fe}_3\text{O}_4/\text{polyacrylonitrile (PAN)}]/[\text{Eu}(\text{BA})_3\text{phen/PAN}]$ nanofiber yarn [29], $\text{Fe}_3\text{O}_4/\text{PANI/PAN}/[\text{Eu}(\text{BA})_3\text{phen/PAN}]$ nanofiber yarn [30], PLLA/n-TCP nanofiber yarn [31], have been successfully prepared by oppositely charged electrospinning. Those nanofibers exhibit high tensile strength, adjustable functional performance and good cell compatibility. In addition, some of 3D-microstructured nanofiber network have been successfully fabricated. Li *et al.* [32] developed an oppositely charged set-up, and thereby a highly intertwined and 3D isotropic network structure was made. Tong *et al.* [33] developed a technique which involved simultaneously positive voltage electrospinning and negative voltage electrospinning to construct nanofiber scaffolds with a rapid increase in thickness. Chang *et al.* [34] used oppositely charged jets to make self-assembly 3D nanofiber networks.

From the oppositely charged electrospinning studies abovementioned, It can be found that the peculiarity of conjugate electrospinning was due to that the nanofibers produced from different nozzles could be bonded together, and the charge was neutralized when they encountered each other. Inspired by this, we propose that the oppositely charged electrospinning present substantial potentials to control the multi-nozzle electrospinning deposition. In this study, a set-up based on the oppositely charged electrospinning was designed, where the air flow was used to transport the neutralized nanofibers. This electrospinning method was named oppositely charged and air auxiliary electrospinning (OCAAES). The concentrated effect of OCAAES was shown first, and the deposition area and pattern controlling of multi-nozzle OCAAES were studied.

Experimental

OCAAES Setup and Working Principle

Figure 1 illustrates the schematic diagram of OCAAES

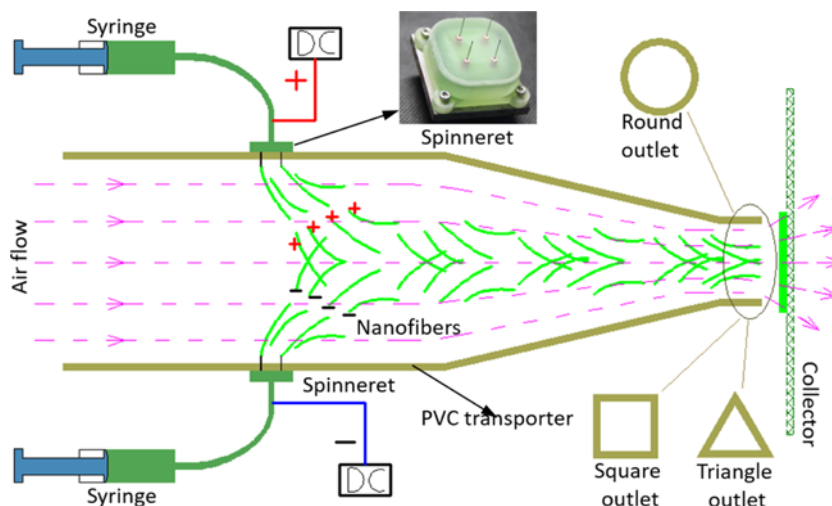


Figure 1. Schematic diagram of the OCAAES.

setup, which includes two syringes, two high-voltage sources (DW-P403-1AC, Tianjing Dongwen, China, one is positive, the other is negative), two spinnerets (single nozzle or four nozzles for each spinneret; stainless needle was used as nozzle with an inner and outer diameter of 210 μm and 400 μm , respectively), a fiber transporter and a nonwoven collector. The polymer solution was transferred from the syringes to the spinnerets by a precision syringe pump (Harvard11 Pico Plus, USA), which was not illustrated in Figure 1. The two spinnerets were face-to-face placed, one of which was connected to the positive high-voltage source, and the other was connected to the negative high-voltage source. The nanofiber transporter was made of PVC (Polyvinyl chloride), and there were some holes in its wall to allow the stainless needles to pass through.

For the OCAAES, when the positive and negative high-voltage sources were turned on, electric field was formed in the space between the two spinnerets. The positively charged jets and negatively charged jets were generated on two spinnerets respectively. Driven by the electric field, the two polarity charged jets moved to each other (due to positive charge moving along electric field line direction and negative charge moving against electric field line direction). The two polarity charged jets were also stretched, and the diameter of charged jets decreased rapidly and then two polarity charged nanofibers was formed. The air flow blew away the charged nanofibers from the high electric field area near the needle to the low electric field space. Thus, the nanofibers was then less influenced by the electric field (namely the relative electric field decreased). As shown in Figure 1 and Figure S1, polymer jets and nanofibers were affected by both airflow and electric field. The air flow provided horizontal power and electric field tended to provide vertical direction power. The air flow pushed nanofibers to the collector and the horizontal velocity of nanofibers was equal to the velocity of air flow. Under the

influence of electric field, nanofibers moved to the axis of symmetry (as shown in Figure S1). The vertical velocity of nanofibers was provided by the electric field. For different nanofibers, the thicker nanofibers had smaller vertical velocity than the finer nanofibers did. The diameter of nanofibers was fluctuant during the electrospinning process. Thus there were three main models for the oppositely charged nanofibers to be touched each other (as shown in Figure S1). When the diameter of the positively charged nanofibers was equal to the diameter of the negatively charged nanofibers, they would touch each other at the axis of symmetry (Figure S1(a)). When the diameter of the positively charged nanofiber was larger than the diameter of negatively charged nanofibers, they would touch each other at the place closer to the positive charge spinneret (Figure S1(b)). When the diameter of the positively charged nanofibers was smaller than the diameter of the negatively charged nanofibers, they would touch each other at the place closer to the negative charge spinneret (Figure S1(c)). The oppositely charged nanofibers were neutralized after they touched each other, and thereafter the electric field stopped driving them. Ultimately most of the nanofibers were moving along with the air flow, thereby nanofibers were deposited on different places of the nonwoven collector consequently.

Material Preparation and Electrospinning Process

Both PI (polyimide) solution and PVA (polyvinyl alcohol) solution were used in this study. PI and dimethylacetamide (DMAc) mixture (with 20 wt.% PI) was purchased from

Hangzhou Surmount Science & Technology (Hangzhou, China). A sufficient mixing by magnetic stirring was conducted for 2 h before electrospinning.

For the eight-nozzle OCAAES, a pair of four-nozzle spinnerets were used. A PVC tube with a diameter of 10 cm was used as the nanofiber transporter. The round shape, square shape and triangle shape outlets were used to fabricate the nanofiber mats in different shapes. The distance between the two spinnerets was 9.6 cm, and the applied voltage was ± 10 kV. The air flow rate was modulated by an air blower (HG-250B) and a speed-control switch, which was measured by an anemograph (UT363). The polymer solution was pumped by the precision syringe pump (Harvard11 Pico Plus, USA, not shown in Figure 1) with a flow rate of 400 $\mu\text{l}/\text{h}$, respectively. Besides, a nonwoven was used as the collector. The collecting time of all the nanofiber mats was fixed to 4 min.

For the two-nozzle OCAAES, a pair of single-nozzle spinnerets were used. A PVC tube with a diameter of 4 cm was used as the nanofiber transporter, and the outlet of the transporter was 4 mm. The distance between the spinnerets was 3.6 cm, and the diameter of the round outlet was 4 mm. The solution flow rate of each spinnerets was 100 $\mu\text{l}/\text{h}$, the air flow rate was 6 m^3/h , and the applied voltage was ± 5 kV. A nonwoven was used as the collector, the distance between the collector and the outlet was 3 mm.

All experiments of this study were performed under ambient conditions with a relative humidity of around 40 % R_H and a temperature of 25 $^\circ\text{C}$.

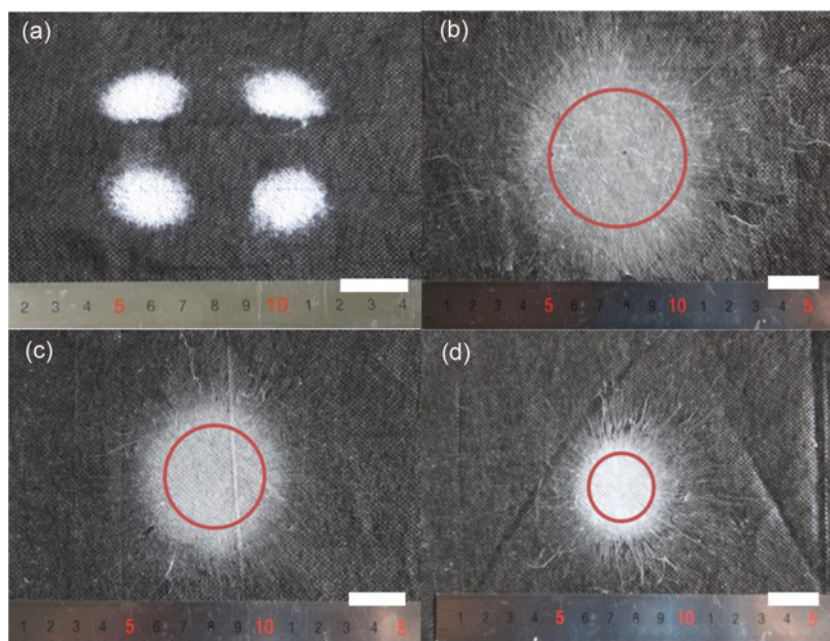


Figure 2. (a) Optical image of the nanofiber mats produced by the conventional electrospinning of four-nozzle spinneret, (b-d) optical images of the concentrated nanofiber mat fabricated by the eight-nozzle OCAAES with round outlets, the outlet diameters were 5.5 cm, 4 cm, 2.5 cm respectively. Note the red marked circles are the section of the round outlet. All the scale bars are 2 cm.

Results and Discussion

To show the concentrated effect of OCAAES in controlling the deposition area of multi-nozzle electrospinning, the results of eight-nozzle OCAAES and four nozzles conventional electrospinning were compared as shown in Figure 2. Due to the repulsions from the neighbor jets by conventional electrospinning, four independent nanofiber areas were obtained, see Figure 2(a). The nanofibers mat fabricated by eight-nozzle OCAAES with round outlets were shown in Figure 2(b)-(d), they are continuous and concentrated rather than randomly separated. The outlet diameters were 5.5 cm, 4 cm, 2.5 cm respectively, and the diameters of the nanofibers mats were correspondingly around 7 cm, 5.5 cm, 4 cm, respectively, as shown in Figure 2(b)-(d). It is obvious that the areas of nanofibers mats decreased with the decreasing diameters of transporter outlets. A few nanofibers were founded in the external area of the red circles due to the air flow flowed outwards after reaching the collector. According to the previous studies of the multi-nozzle electrospinning controlling [23-25], the electrospinning deposition area could decrease only in a limited range, the electrospinning deposition could not produce a continuous web in several minutes. As a comparison, continuous nanofiber mats were fabricated via multi-nozzle OCAAES immediately at the beginning. In addition, the concentrated nanofiber mats could be fabricated by decreasing the diameter of transporter outlet.

To show the morphological characteristics of OCAAES nanofibers and conventional electrospinning nanofibers,

OCAAES of a pair of single nozzle spinnerets and conventional electrospinning of single nozzle spinneret were used to fabricate the nanofibers (the fabrication processes and characterization process were presented in the supplementary information). The microstructure of the nanofibers fabricated by conventional electrospinning and OCAAES was shown in Figure 3. It can be seen from Figure 3(a) and d some spindle structures were found in the nanofibers. The diameter of spindle structures was 1-4 μm , however, the spindle structures were not taken into consideration when calculating the diameter of the nanofibers. The average diameter of conventional electrospinning nanofibers was 103.3 nm, while that for OCAAES ones was 147.4 nm. In the OCAAES process, although the jets were additionally stretched by airflow, the diameter of nanofibers produced from OCAAES method was still larger than that of conventional electrospinning. The electric field distribution of conventional electrospinning and OCAAES was shown in Figure S2. We found that the electric field intensity of conventional electrospinning was higher and the electric field was more uniform. It has been reported that even electric field with a higher intensity could produce finer fiber during electrospinning process [17,18]. Therefore the larger diameter of OCAAES nanofibers may arise from the uneven electric field with lower intensity.

The initial velocity of the electrospinning jet was approximately 0.05-0.5 m/s [36,37]. The airflow in electrospinning process provided an additional stretching force on the jet. Especially, when the velocity of airflow was larger than that of the initial charged jet. The relative

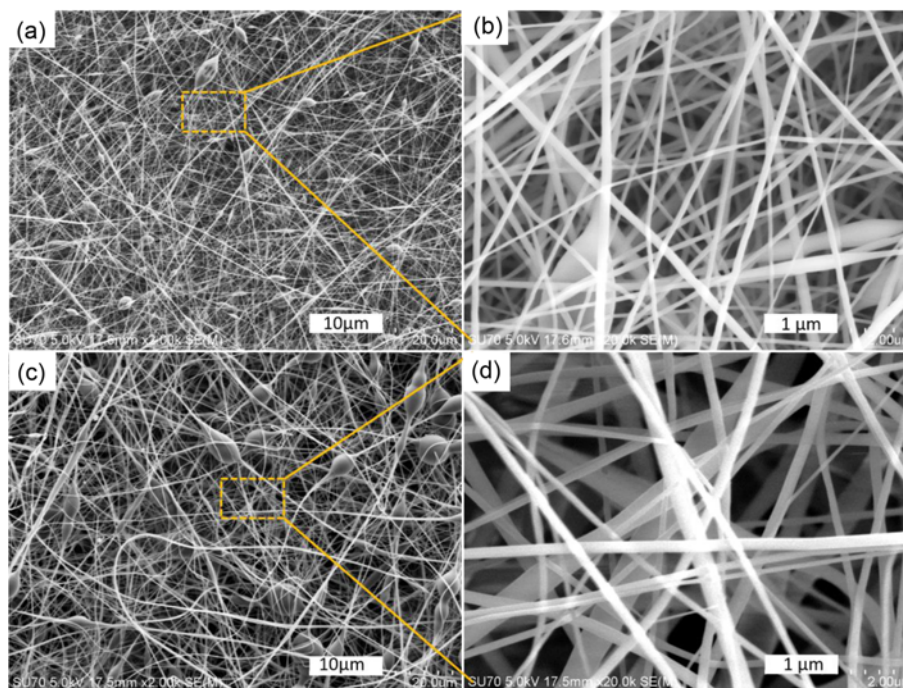


Figure 3. SEM images of the PI nanofibers fabricated by conventional electrospinning (a, b) and OCAAES (c, d) respectively.

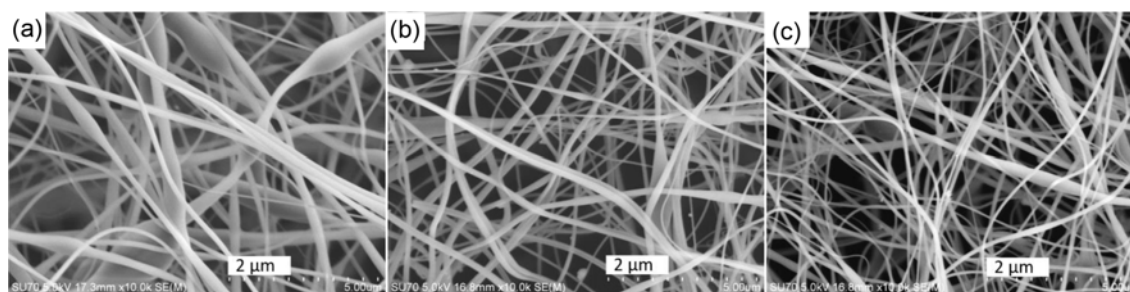


Figure 4. SEM images of the PI nanofiber microstructure fabricated by OCAAES with different airflow rates acting on the initial jets; (a) 1 m/s, (b) 2 m/s, and (c) 3 m/s.

velocity between the airflow and charged jet was the primary reason for the additional stretching force [37]. For OCAAES, the airflow was perpendicular to the spinneret, thus a relative velocity between the airflow and the initial jet was formed. The stretching force of jet increased with the increasing airflow speed. Figure 4 shows the microstructure of nanofibers produced at different airflow rates. In the experiments, the airflow rate of the outlet was measured. The airflow rates of the outlet were 6.25 m/s, 12.5 m/s and 18.75 m/s, respectively. The diameter of outlet and the PVC transporter were 4 cm and 10 cm, so the airflow of the PVC transporter was 1/6.25 of that of the outlet. The airflow of the PVC transporter was the airflow rate acting on the initial jets, which were then determined as 1 m/s, 2 m/s and 3 m/s, respectively, in Figure S4(a-c). The diameter of nanofibers was reversely proportional to the increase in the airflow rate. As shown in Figure 4, with the increasing airflow, the average diameters of nanofibers were 170.2 nm, 147.4 nm and 114.5 nm, respectively. This is because a higher airflow rate provided a stronger additional stretching force acting on the jets, resulting in thinner nanofibers. The effect of the airflow of the outlet on nanofiber mat size was studied as well. The airflow rate of the outlet were 6.25 m/s, 12.5 m/s and 18.75 m/s, respectively. As shown in Figure S3, the diameter of nanofiber mat was around 6.2 cm and almost did not change with the airflow.

By use of the eight-nozzle OCAAES, the patterned nanofiber mat could be fabricated as well. As can be seen from Figure 5, two patterned nanofiber mats were formed in the shape of square and regular triangle, respectively. For Figures 5(a) and (b) the distance between the collector and the nanofibers transporter outlet was 3 cm. The square nanofiber mat was obtained by using the square nanofibers transporter outlet (the length of the side of the cross-section of the outlet was 4 cm). The regular triangle nanofiber mat was obtained by using the regular triangle nanofibers transporter outlet (the length of the side of the cross-section of the outlet was 5 cm). The areas of the patterned nanofibers mats were larger than that of the cross-section of fibers transporter outlet, which was because the air flow flowed outwards after reaching the collector.

To fabricate superior patterned nanofibers mats, that all air

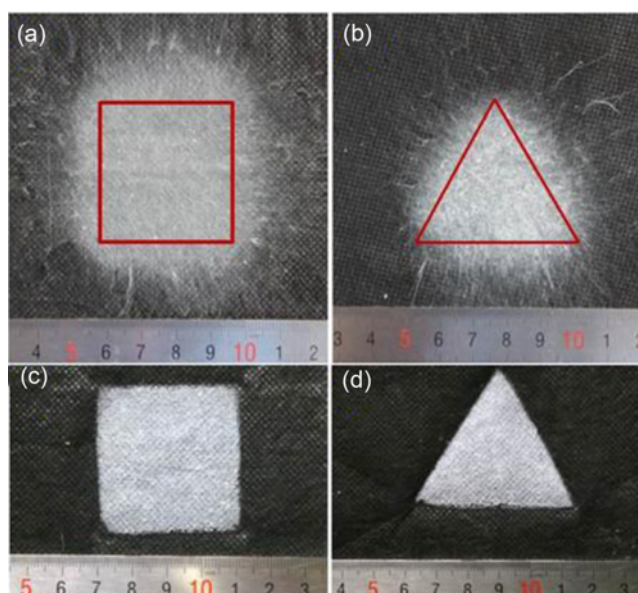


Figure 5. Optical images of patterned nanofibers mats; (a) and (c) nanofiber mats fabricated by a square outlet, (b) and (d) nanofiber mats fabricated by a triangle outlet. Note the marked red circles are the section of outlets.

flow passed through the nonwoven collector was needed. As a result, we fixed the nonwoven collector on the nanofibers transporter outlet. Square outlet (the length of side was 4 cm) and regular triangle outlet (the length of side was 5 cm) were used to fabricate the patterned nanofiber mats. The fabricated patterned nanofibers mats were shown in Figures 5(c) and (d). It can be found that the patterns of the mats duplicated the shapes of the transporter outlet. Therefore, the multi-nozzle mat pattern can be controlled by designing the outlet shape and changing the distance between the outlet and the collector.

We have confirmed that concentrated and patterned nanofiber mat could be fabricated by OCAAES. To further demonstrate that concentrated nanofiber deposition could be fabricated with a quicker thickening rate, a round nanofiber transporter outlet with a diameter of 4 mm was used in the two-nozzle OCAAES. Figures 6(a) and (b) show the static

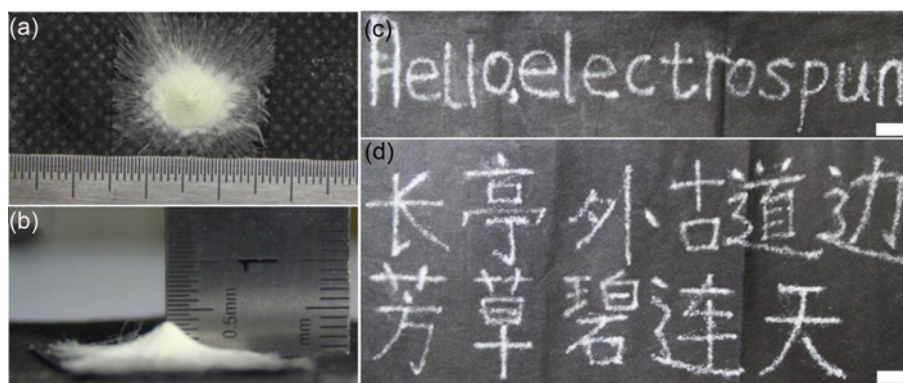


Figure 6. Optical images of nanofiber taper and hand-written characters; (a) nanofiber taper deposited on a fixed collector by OCAAES in ten minutes, (b) the lateral view of (a), (c) some English words written by manually controlling the motion of collector in 2 min and (d) a Chinese sentence was directly written within 6 min. Note the scale bars of (c) and (d) were 2 cm.

deposition results of OCAAES. Clearly the height of the taper increased to 4 mm in only 10 minutes. The deposition area was concentrated by OCAAES, and the base cycle diameter of the nanofiber taper was around 10 mm. It is known that 2D nanofiber mats were commonly made by the conventional electrospinning. Considering that the nanofiber mat area increases with time, it is thus difficult to fabricate thick nanofiber deposition by the conventional electrospinning. For example, Mi *et al.* [35] employed a conventional electrospinning set-up which contained a rotating collector to fabricate the nanofiber. It in fact took 18 hours to fabricate an 1144.9 μm thick nanofiber scaffold. Therefore, compared with the conventional electrospinning, OCAAES could fabricate nanofiber deposition in a quicker thickening rate.

Based on the concentrated effect of OCAAES, the deposition pattern of multi-nozzle electrospinning could be controlled actively. The two-nozzle OCAAES with round transporter outlet with a diameter of 4 mm was used to directly write nanofiber patterns. The movement of the collector was controlled manually to write nanofiber patterns. When the collector was moved along the trajectory 'Hello, electrospun' with a speed about 7 mm/s using a circular outlet, the same patterns (as shown in Figure 6(a)) almost concurrently appeared on the nonwoven collector within 2 minutes. As an illustration, a Chinese famous sentence from an ancient poem was also successfully fabricated in 6 minutes, see Figure 6(b). Therefore, by decreasing the diameter of round transporter outlet to millimeters level, the OCAAES set-up could play a role like a brush. The arbitrary patterned nanofiber deposition could be fabricated accordingly, therefore the pattern of nanofiber mat could be controlled actively by the OCAAES.

Conclusion

To effectively control multi-nozzle electrospinning deposition, an oppositely charged and air auxiliary electrospinning

(OCAAES) device was designed. Experimental results indicated that the concentrated and patterned nanofiber deposition was successfully fabricated by the OCAAES. Based on the concentrated effect of OCAAES, the nanofiber deposition area of multi-nozzle electrospinning could be controlled actively, while the nanofiber deposition could be fabricated in a quick thickening rate. The deposition patterns of multi-nozzle electrospinning were controlled actively as well (the OCAAES set-up could function as a brush, and arbitrary patterned nanofiber deposition could be fabricated). It can be concluded that the OCAAES is a simple yet powerful method in controlling the multi-nozzle electrospinning nanofiber deposition. In this study, we only present the capability of OCAAES in controlling the multi-nozzle electrospinning nanofiber deposition, but OCAAES also holds excellent promises in controlling the free surface electrospinning.

Acknowledgments

This work was supported by the National Natural Science Foundation of China (U1505243, 51475398 and 91648114).

Electronic Supplementary Material (ESM) The online version of this article (doi: 10.1007/s12221-019-8984-y) contains supplementary material, which is available to authorized users.

References

1. C. Kim, B. T. N. Ngoc, K. S. Yang, M. Kojima, Y. A. Kim, Y. J. Kim, M. Endo, and S. C. Yangite, *Adv. Mater.*, **19**, 2341 (2007).
2. Y. Z. Feng, I. S. Cho, P. M. Rao, L. L. Cai, and X. Zheng, *Nano Lett.*, **13**, 855 (2013).
3. Y. Xia, *Nat. Mater.*, **7**, 758 (2008).
4. Y. Z. Zhang, C. T. Lim, S. Ramakrishna, and Z. M. Huang,

- J. Mater. Sci-Mater. M.*, **16**, 933 (2005).
5. K. T. Shalumon, S. Deepthi, M. S. Anupama, S. V. Nair, R. Jayakumar, and K. P. Chennazhi, *Int. J. Biol. Macromol.*, **72**, 1048 (2015).
 6. Q. Wang, Y. Bai, J. Xie, Q. Jiang, and Y. Qiu, *Powder Technol.*, **292**, 54 (2016).
 7. H. Wan, N. Wang, J. Yang, Y. Si, K. Chen, B. Ding, G. Sun, M. El-Newehy, S. S. Al-Deyab, and J. Yu, *J. Colloid Interf. Sci.*, **417**, 18 (2014).
 8. N. Wang, Y. Si, N. Wang, and G. Sun, *Sep. Purif. Technol.*, **126**, 44 (2014).
 9. Y. Yang, S. Zhang, X. Zhao, J. Yu, and B. Ding, *Sep. Purif. Technol.*, **152**, 14 (2015).
 10. S. Zhang, N. Tang, L. Cao, X. Yin, J. Yu, and B. Ding, *ACS Appl. Mater. Inter.*, **8**, 29062 (2016).
 11. C. Shi, P. Z. Zhang, S. H. Huang, P. T. Yang, D. Z. Wu, D. H. Sun, and J. B. Zhao, *J. Power Sources*, **298**, 158 (2015).
 12. D. Z. Wu, C. Shi, S. H. Huang, X. C. Qiu, H. Wang, Z. Zhan, P. Zhang, J. B. Zhao, D. H. Sun, and L. W. Lin, *Electrochim. Acta*, **176**, 727 (2015).
 13. Y. Yang, Z. Jia, L. Hou, J. Liu, L. Wang, and Z. Guan, *IEEE Trans. Dielect. Electr. Insul.*, **17**, 1592 (2010).
 14. G. H. Kim, Y. S. Cho, and W. D. Kim, *Eur. Polym. J.*, **42**, 2031 (2006).
 15. L. Tian and C. C. Zhao, *Sci. Adv. Mater.*, **7**, 2327 (2015).
 16. Y. S. Zheng, X. K. Liu, and Y. C. Zeng, *J. Appl. Poly. Sci.*, **130**, 3221 (2013).
 17. Y. S. Zheng, S. Xie, and Y. C. Zeng, *J. Mater. Sci.*, **48**, 6647 (2013).
 18. Y. S. Zheng, C. M. Zhuang, R. H. Gong, and Y. C. Zeng, *Ind. Eng. Chem. Res.*, **53**, 14876 (2014).
 19. D. H. Sun, X. C. Qiu, Z. Q. Xu, X. W. Hu, G. Q. He, L. W. Lin, and D. Z. Wu, *Nanotechnol. Precis. Eng.*, **11**, 391 (2013).
 20. K. M. Forward and G. C. Rutledge, *Chem. Eng. J.*, **183**, 492 (2012).
 21. I. Bhattacharyya, M. C. Molaro, R. D. Braatz, and G. C. Rutledge, *Chem. Eng. J.*, **289**, 203 (2016).
 22. S. A. Theron, A. L. Yarin, E. Zussman, and E. Kroll, *Polymer*, **46**, 2889 (2005).
 23. Y. Yang, Z. D. Jia, L. Hou, Q. Li, L. M. Wang, and Z. C. Guan, *IEEE Trans. Dielectr. Electr. Insul.*, **15**, 269 (2008).
 24. Y. Yang, Z. D. Jia, and Z. C. Guan, *IEEE Intern. Conf. Dielectric Liquids*, p.457, 2005.
 25. S. Xie and Y. C. Zeng, *Ind. Eng. Chem. Res.*, **51**, 5336 (2012).
 26. J. He, K. Qi, Y. Zhou, and S. Cui, *Polym. Int.*, **63**, 1288 (2014).
 27. J. He, Y. Zhou, Y. Wu, and R. Liu, *Surf. Coat. Technol.*, **258**, 398 (2014).
 28. J. He, K. Qi, L. Wang, Y. Zhou, R. Liu, and S. Cui, *Fiber. Polym.*, **16**, 1319 (2015).
 29. L. Fan, Q. Ma, J. Tian, D. Li, X. Xi, X. Dong, W. Yu, J. Wang, and G. Liu, *J. Mater. Sci.*, **53**, 2290 (2018).
 30. L. Fan, Q. Ma, J. Tian, D. Li, X. Xi, X. Dong, W. Yu, J. Wang, and G. Liu, *RSC Adv.*, **7**, 48702 (2017).
 31. X. Li, C. Yao, F. Sun, T. Song, Y. Li, and Y. Pu, *J. Appl. Polym. Sci.*, **107**, 3756 (2008).
 32. M. Li, Y. D. He, C. L. Xin, X. P. Wei, Q. C. Li, and Y. J. Juang, *Appl. Phys. Lett.*, **92**, 213114 (2008).
 33. H. Tong and M. Wang, *Mater. Lett.*, **94**, 116 (2013).
 34. G. Q. Chang, X. F. Zhu, A. K. Li, W. W. Kan, R. Warren, R. G. Zhao, X. L. Wang, G. Xue, J. Y. Shen, and L. W. Lin, *Mater. Des.*, **97**, 126 (2016).
 35. S. Mi, B. Kong, Z. Wu, W. Sun, Y. Xu, and X. Su, *Mater. Lett.*, **160**, 343 (2015).
 36. G. Zheng, L. Sun, X. Wang, J. Wei, L. Xu, Y. Liu, J. Zheng, and J. Liu, *Appl. Phys. A: Mater.*, **122**, 112 (2016).
 37. Y. Zhao, J. Jiang, W. Li, X. Wang, K. Zhang, P. Zhu, and G. Zheng, *AIP Adv.*, **6**, 115022 (2016).